Ordering of Cylindrical Domain of Block Copolymers under Moving Temperature Gradient: Effects of Moving Rate

Kazuki Mita,[†,‡] Hirokazu Tanaka,[†,‡] Kenji Saijo,[†] Mikihito Takenaka,[†,§] and Takeji Hashimoto*[,†,||]

Department of Polymer Chemistry, Graduate School of Engineering, Kyoto University, Katsura, Nishikyo-ku, Kyoto 615-8510, Japan, Structural Materials Science Laboratory, SPring-8 Center, RIKEN Harima Institute Research, Hyogo 679-5148, Japan, and Advanced Science Research Center (ASRC), Japan Atomic Energy Agency (JAEA), Tokai-mura, Ibaraki-Pref. 319-1195, Japan

Received January 28, 2008; Revised Manuscript Received April 17, 2008

ABSTRACT: In a previous paper (*Macromolecules* 2007, *40*, 5923), we reported that a zone heating method, which imposes the moving temperature-gradient (∇T) field on ordering process of various melts in general, enabled to control a macroscopic orientation of hexagonally packed cylindrical microdomain structures (hex-cyl) of block copolymer (bcp) bulk. In this report, we have investigated how the variation of the moving rate of ∇T affects the macroscopic orientation by using two kinds of polystyrene-*block*-polyisoprene bcps having different mobility. We found that the upper limit of the moving rate required to induce the unique texture and orientation of hex-cyl became large with increasing the mobility of the bcps. These results indicate that the moving rate should be smaller than the intrinsic growth rate of the hex-cyl grains in the undercooled disordered melt.

1. Introduction

In our previous paper,[1] we have reported a control of the macroscopic orientation of hexagonally packed cylindrical microdomain structure (hex-cyl) by using a zone heating method. In this method, we imposed a moving temperature gradient (∇T) on polystyrene-*block*-polyisoprene (SI) diblock copolymer (dibcp) during its ordering process from the disorder state to hex-cyl of polystyrene (PS) block chains in the matrix of polyisoprene (PI) block chains (PS hex-cyl). The method was found to create the following special texture of hex-cyl: (1) The texture consists of volume-filled columnar grains extended parallel to the ∇T axis (defined as the Oz axis); (2) The cylinder axis within any grains always orients perpendicular to Oz with a rotational angle ϕ of the cylinder axis around Oz being fixed within a grain but statistically varying randomly among different grains; (3) The (100) plane of hex-cyl preferentially oriented perpendicular to Oz with a small rotational degree of freedom around the cylinder axis.

In this work, we address the question on whether or not we can develop the same texture as mentioned above when the zone heating method is applied to a dibcp forming "reversed" hex-cyl, that is, hex-cyl of PI block chains in the matrix of PS block chains (PI hex-cyl). More specifically, we address a question how the displacement rate R of ∇T should be optimized with respect to the mobility of the dibcps at order−disorder transition (ODT) temperature T_{ODT} in order to create the special texture.

In the zone heating method employed in this experiment as well as in the previous experiment,[1] a bulk bcp specimen fixed in the cell contacts a glass surface set perpendicular to the Oz axis (Figure 1a). A temperature gradient ∇T and its moving direction was set along the Oz direction in such a way that $\nabla T = 0$ for $T \le T_1$ and $T \ge T_2$ and $\nabla T =$ (a positive constant) for $T_1 \le T \le T_2$. The T_{ODT} exists between T_1 and T_2 ($T_1 \le T_{ODT} \le T_2$). The edge of the ∇T zone having a higher temperature continuously moves from the glass surface side of the specimen to the opposite side of the specimen along the Oz direction. The entire specimen is initially in disordered state. Then, as ∇T moves along the Oz axis, ordering occurs sequentially from the glass surface side toward the interior of the specimen. As detailed previously,[1] this sequential ordering is strongly affected by the surface-induced ordering of block copolymers (bcps), for which the glass surface plays a role in the early stage of zone heating. In the rest of the stage, the surface of as-grown, well-aligned microdomain structure plays a role for the surface-induced ordering in place of the glass surface. In order to bring about the sequential ordering, the conditions of a large ∇T and a small gradient displacement rate R are required so that the ordering occurs only in a supercooled disorder phase existing in a very narrow slitlike space where temperature is below T_{ODT} as will be detailed below; the width of the gradient zone is typically about 1 mm. Otherwise, the specimen would have a wide region of supercooled disordered melt where a random nucleation and growth of microdomains will occurs.

Whether or not the ordering occurs only in the slitlike space depends on a time span over which molten bcps are allowed to stay in the slitlike space, Δt_s, and time for completing the surface-induced ordering, Δt_o. When Δt_o is smaller than Δt_s ($\Delta t_o < \Delta t_s$), the ordering occurs only in the slitlike space and the sequential ordering under moving ∇T will be achieved. Obviously $\Delta t_s \sim R^{-1}$ and $\Delta t_o \sim G^{-1}$ where G is the growth rate of grains having ordered microdomains of bcps. Consequently a small value of R and/or a large value of G are required to form macroscopically well-aligned microdomain structure. G depends on mobility of molten bcps.

The mobility of the bcps forming the PI hex-cyl is lower than that of the bcps forming the PS hex-cyl, if the two bcps have the same molecular weight, because the content of PS block chains is higher in the former than that in the latter. In this work, we shall explore how the change in mobility affects the orientation of hex-cyl by the zone-heated PI hex-cyl specimens and compare the results with those previously obtained for the zone-heated PS hex-cyl specimens. Furthermore, we shall clarify effects of R on the macroscopic orientation of hex-cyl.

* To whom correspondence should be addressed.
[†] Department of Polymer Chemistry, Graduate School of Engineering, Kyoto University.
[‡] Present address; R&D Center, Mitsui Chemicals, Inc., 580-32 Nagaura, Sodegaura, Chiba 299-0265, Japan.
[§] Structural Materials Science Laboratory, SPring-8 Center, RIKEN Harima Institute Research.
[||] Advanced Science Research Center (ASRC), Japan Atomic Energy Agency (JAEA).

10.1021/ma8001998 CCC: $40.75
Published on Web 08/22/2008

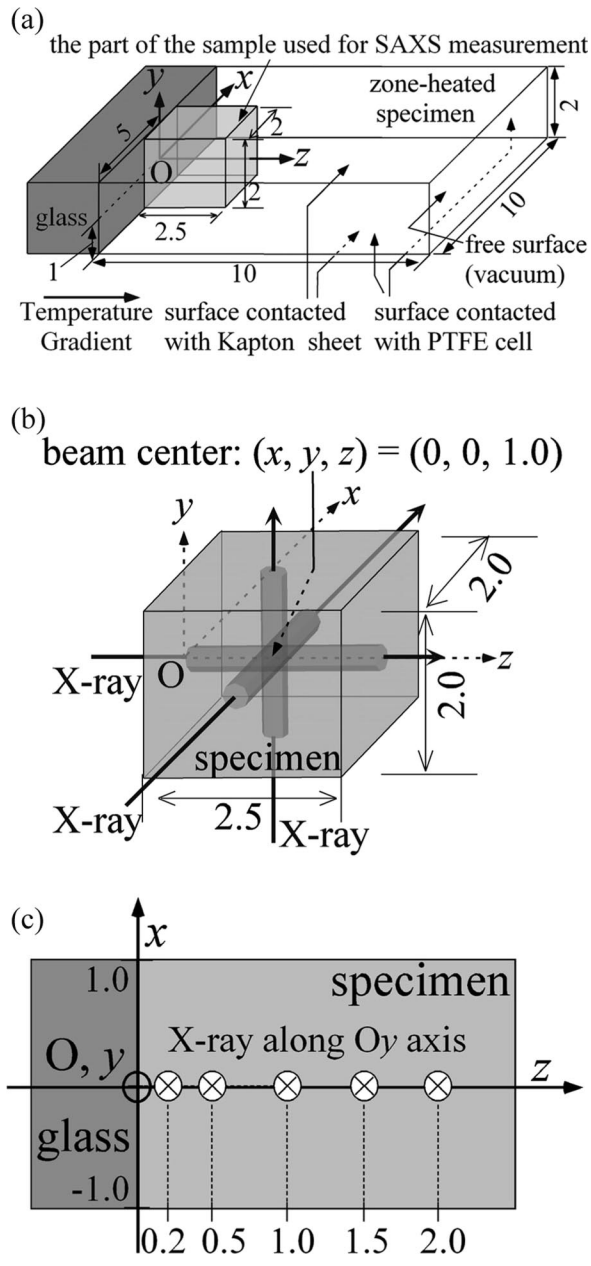

Figure 1. Schematic diagram showing geometric relationships among incident X-ray beam, the specimen and the Cartesian coordinate. The lengths in this figure are expressed in units of millimeters. During the zone heating process, the film specimen was placed inside the cell made out of polytetrafluoroethylene (PTFE) with a glass surface on one end of the specimen surface (a). Thin Kapton sheets were placed on both side of the specimen surface parallel to the Oxz plane. The origin of the Cartesian coordinate was set to be the center of the glass surface (a). The cube of the specimen shown in part b corresponds to that shaded with light gray in part a and was cut out from the frozen, zone-heated specimen for SAXS measurements. The incident X-ray beams were irradiated from three orthogonal directions along x, y, and z directions through a common center of (0, 0, 1.0) (b). The position of incident beam along the Oy direction was changed along the z direction, keeping $x = 0$ (c).

2. Experimental Method

2.1. Sample. Two kinds of samples were used as specimens. One was a neat SI dibcp (coded as YM-1), whose characteristics are summarized in Table 1. The other was a blended sample of SI dibcp (coded as SI-1) and homopolyisoprene (coded as HI) with a blending ratio of SI-1/HI = 95/5 in wt%, which was designated as SI-1/HI(95/5). The characteristics of SI-1, HI and SI-1/HI(95/5) are also summarized in Table 2. Since the scattering maximum from

Table 1. Characteristics of the Sample Used as the Low Mobility System[a]

code	M_n	M_w/M_n	f_{PI}	T_{ODT} (°C)	D_{100} (nm)
YM-1	2.3×10^4	1.04	0.31	147	18

[a] M_n: number-average molecular weight estimated by GPC; M_w/M_n: polydispersity index where M_w is weight-average molecular weight measured by gel permeation chromatography (GPC), f_{PI}: volume fraction of polyisoprene estimated by using M_n of each block, and assuming densities of PS and PI in the system to be equal to those of corresponding homopolymers;[18,19] T_{ODT}: order-disorder transition temperature evaluated by SAXS; D_{100}: Bragg spacing of hex-cyl.

Table 2. Characteristics of the Samples Used as the High Mobility System[a]

code	M_n	M_w/M_n	f_{PS}	T_{ODT} (°C)	D_{100} (nm)
SI-1	3.1×10^4	1.01	0.33	191	
HI	1.2×10^3	1.08	0		
SI-1/HI(95/5)			0.31	178	22

[a] f_{ps} volume fraction of polystyrene estimated by using M_n of each block in SI-1 and that of HI, and assuming densities of PS and PI in the system to be equal to those of corresponding homopolymers.[18,19]

(110) plane of hex-cyl of the neat SI-1 is suppressed because of its special volume fraction of PS,[1,2] and the suppression makes the analyses of the orientation of hex-cyl difficult, we blended HI into SI-1 in order to enhance the (110) scattering intensity. As shown in the Appendix, mobility of YM-1 is lower than that of SI-1/HI(95/5), and thus we designated "low mobility (PI hex-cyl)" and "high mobility (PS hex-cyl)" for YM-1 and SI-1/HI(95/5), respectively. Each sample was mixed with antioxidant (Irganox1010) and cast from a homogeneous solution in toluene with a total polymer concentration of 10 wt %, and then annealed in vacuum at 120 °C for 8 h.

The as-cast film of YM-1 had a PI hex-cyl, while that of SI-1/HI(95/5) had a PS hex-cyl where HI is expected to be uniformly distributed in the matrix of PI block chains.[3] The small-angle X-ray scattering (SAXS) experiment was conducted to evaluate the Bragg spacing and T_{ODT} of YM-1 and SI-1/HI(95/5) in the same way as detailed previously.[1] The Bragg spacings of YM-1 and SI-1/HI(95/5) corresponding to (100) plane, D_{100}, were 18 and 22 nm, respectively, and the T_{ODT} values of YM-1 and SI-1/HI(95/5) were at 147 and 178 °C, respectively.

2.2. Zone Heating. We used the "zone heating device" described in detail elsewhere[1] in order to impose moving ∇T on the specimens. In this experiment, a sharp nominal temperature gradient of $|\nabla T|_{nom} = 62$ °C/mm with T_2 and T_1 being 190 and 5 °C, respectively, was used for YM-1, and $|\nabla T|_{nom} = 73$ °C/mm with T_2 and T_1 being 225 and 5 °C, respectively, for SI-1/HI(95/5). Each ∇T crosses the T_{ODT} of each sample. The widths of the gradient zone between T_{ODT} and $T_{g,PS} \approx 90$ °C (the glass transition temperature of PS microdomains) are 0.92 and 1.2 mm for YM-1 and SI-1/HI(95/5), respectively.[4] As shown in Figure 1a, we set the Cartesian coordinate Oxyz fixed to the specimen with its origin right in the middle of the glass surface. The glass surface set parallel to Oxy plane was contacted with the specimen. We used a polystyrene (PS)-coated glass surface for YM-1, and a bare glass (soda-lime glass) surface for SI-1/HI(95/5). The role of the glass-surface treatment will be clarified later in section 4.4. The preparation method of PS-coated glass surface was described elsewhere.[5,6] The temperature gradient was set and moved along the Oz direction. Moving rates R employed were listed in Table 3. $R = 75$ nm/s was the slowest velocity for SI-1/HI(95/5), which was determined by a trial and error method under the condition where thermal degradation of the specimen is effectively insignificant.[1] In Table 3, R was expressed in the unit of D_{100} also; e.g., $R = 75$ nm/s $= 3.4$ D_{100}/s in order to help an intuitive visualization of the rate R.

The effective temperature gradient $|\nabla T|_{eff}$ was determined as detailed elsewhere[1] by measuring temperature at a given point in the specimen with a thermocouple embedded in it as a function of time for each condition. Thus evaluated $|\nabla T|_{eff}$ values were much smaller than $|\nabla T|_{nom}$, which may be due to conduction of heat within

Table 3. Conditions of Zone Heating and SAXS Experiments[a]

	R		$\|\nabla T\|_{eff}$		SAXS experiments		
sample code	nm/s	D_{100}/s	°C/mm	°C/D_{100}	A	B	remark
YM-1	25	1.4	22	4.0×10^{-4}	H	S	low mobility (PI hex-cyl)
	125	7	22	4.0×10^{-4}		H	
SI-1/HI(95/5)	75	3.4	42	9.2×10^{-4}		S	high mobility (PS hex-cyl)
	125	5.7	42	9.2×10^{-4}		H	
	500	22.7	42	9.2×10^{-4}		H	

[a] H: in-house SAXS apparatus. S: synchrotron radiation SAXS apparatus.

the specimen. We quenched the zone-heated specimen below the glass transition temperature of PI block chains ($T_{g,PI}$) by quickly dunking it into liquid N_2 in order to solidify the structure developed via the zone heating method.

2.3. Small Angle X-ray Scattering. SAXS measurements were conducted at room temperature on the solidified specimen, prepared as described above, cut out into a rectangular parallelepiped shape as shown in Figure 1a. It should be noted here that the polyimide (Kapton) sheets, which contact with the specimens in the yz plane at $y = \pm 1$ mm, were found to hardly affect the specific orientation of hex-cyl developed under the zone heating method as elucidated in the previous paper (see the second paragraph of section 3.3 in ref 1).[7] This fact is also true in the case of macroscopically aligned single crystal-like lamellae texture developed by the zone heating method, as evidenced by the fact the SAXS pattern taken on the q_xq_z plane is essentially identical to that on the q_yq_z plane,[6] although this fact was not explicitly stated in ref 6. Here, q_x, q_y, and q_z are x, y, and z components of the scattering vector **q**, respectively. The specimen extends along the Ox, Oy, and Oz directions, as specified by $-1.0 \le x/\text{mm} \le 1.0$, $-1.0 \le y/\text{mm} \le 1.0$, and $0 \le z/\text{mm} \le 2.5$. We used two SAXS apparatuses, an in-house SAXS apparatus[8] and the synchrotron radiation SAXS apparatus[9] at the BL45XU, SPring-8. The in-house SAXS apparatus was detailed elsewhere[1] so that we shall not repeat the description here.[10] In the synchrotron radiation SAXS apparatus, the wavelength of incident X-ray was 0.1 nm, and 2D SAXS images were obtained with a cooled charge coupled device (CCD) camera[9] having an image-intensifier, and the sample-to-detector distance was 2.3 m. The beam size at the sample surface was square shape of 0.2 mm × 0.2 mm.

As described in Table 3, SAXS experiments designated as "experiment A" were conducted for the YM-1 specimen zone-heated under the condition of the smallest moving rate $R = 25$ nm/s. Although this specimen is characterized as the low mobility system, the orientation of hex-cyl is expected to be well developed with this smallest R, as in the case of the high mobility system with $R = 75$ nm/s.[1]

SAXS experiments designated as "experiment B" were conducted for all the specimens listed in Table 3 in order to clarify the effects of R and mobility of the systems on the orientation of hex-cyl. The effect of R can be clarified by comparing SAXS patterns obtained with specimens subjected to different R for both the low mobility system and the high mobility system. The mobility effect can be discussed by comparing the SAXS patterns obtained for the low mobility system with those for the high mobility system, keeping R at 125 nm/s or keeping R the smallest values ($R = 25$ nm/s for the low mobility system; $R = 75$ nm/s for the high mobility system).

SAXS experiment A was conducted by using the in-house SAXS apparatus, and SAXS experiment B was conducted by using the in-house SAXS apparatus and the synchrotron radiation SAXS apparatus. In each set of 2D SAXS patterns measured by the same apparatus, the scattering intensities were normalized by exposure time.

In SAXS experiment A, the incident beam was irradiated from three orthogonal directions, along the Ox, Oy, and Oz directions, through a common center of (0, 0, 1.0) (Figure 1b) in order to investigate the orientation developed in the low mobility system.[11] In SAXS experiment B, the incident beam was irradiated at different positions along the Oz direction, keeping $x = 0$ and keeping the incident beam irradiated along the Oy direction (Figure 1c) in order to investigate the z-dependence of the orientation for the low and high mobility systems zone-heated at the smallest R. Since the pattern taken with the incident beam along the Oy axis is the same as that along the Ox axis,[1] we indicated the results obtained with the incident beam along the Oy direction only. A point of $z/\text{mm} = 1.0$, $x/\text{mm} = 0$, and $y/\text{mm} = 0$ was chosen as the incident beam position irradiated parallel to Oy axis in order to investigate the effect of R on the orientation of hex-cyl for both the low and high mobility system. The exposure time for taking a 2D SAXS pattern was 50 ms with the synchrotron radiation SAXS apparatus and 7200 s with the in-house SAXS apparatus.

3. Results

3.1. Application of Zone Heating to Low Mobility System. It is not self-evident whether the low mobility system YM-1 can attain the same special texture and orientation of hex-cyl as that found in the previous paper[1] for the high mobility system of SI-1/HI(95/5) zone-heated at $R = 75$ nm/s. Thus we first investigated the texture and orientation of hex-cyl attained for the low mobility system with the zone-heating at the smallest $R = 25$ nm/s. For this purpose we conducted the SAXS experiments in the same manner as in the previous paper.[1] The SAXS patterns taken with incident beam along the Ox, Oy, and Oz were essentially the same as those found for SI-1/HI(95/5) zone heated at $R = 75$ nm/s, as shown separately in the Supporting Information (Supporting Information 1), revealing that the low mobility system also can attain the special texture and orientation inherent in the zone-heating method. Therefore we can advance our research by a step further to investigate the effects of R on the texture and orientation of hex-cyl for the low mobility system.

3.2. Effect of Moving Rate on Orientation of Hex-Cyl. We now extend our studies to explore the effects of R on the orientation of hex-cyl in the low mobility system YM-1 as well as the high mobility system SI-1/HI(95/5). Note that the previous paper dealt with only a single value of $R = 75$ nm/s for the high mobility system. 2D SAXS patterns were taken for the specimens obtained under various zone heating conditions listed in Table 3. The incident beam was irradiated along the Oy direction at a fixed position in the specimens specified by (x/mm, y/mm, z/mm) = (0, 0, 1.0). The corresponding 2D SAXS patterns are shown in Figure 2a−e.

First, we focus on the low mobility system YM-1. As already clarified in the previous paper[1] and described in section 3.1 in this paper, in the case of $R = 25$ nm/s (part a), the (100) and (110) diffractions gave the characteristic scattering patterns from the hex-cyl developed via the zone heating process. On the other hand, in the case of $R = 125$ nm/s (part b), the diffraction from (100) plane becomes almost circular, indicating that the zone heating process with $R = 125$ nm/s did not induce the specific texture and orientation. Thus, there is an upper limit of the moving rate in order to attain the specific texture and orientation of hex-cyl inherent in the zone heating method.

Next, we focus on the high mobility system SI-1/HI(95/5). Parts c and d in Figure 2 ($R = 75$ and 125 nm/s, respectively) exhibit the characteristics of the scattering pattern from the hex-cyl developed via the zone heating process. On the other hand,

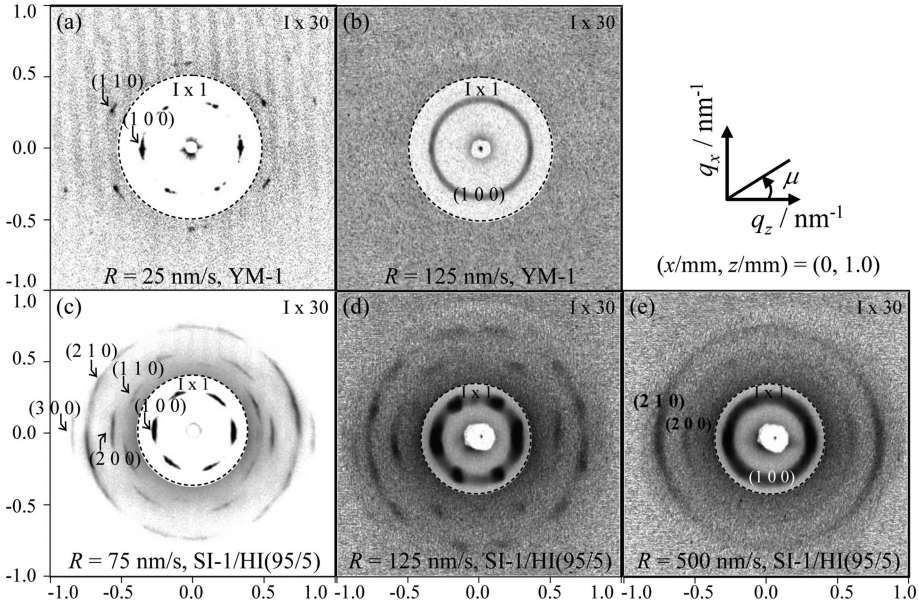

Figure 2. Moving-rate R dependence of 2D SAXS patterns in the q_xq_z plane at $x = 0$ mm, $y = 0$ mm, and $z = 1.0$ mm (experiment B). key: (a) $R = 25$ nm/s and (b) 125 nm/s for the low mobility system YM-1; (c) $R = 75$ nm/s, (d) 125 nm/s, and (e) 500 nm/s for the high mobility system SI-1/HI(95/5). The intensity outside of the dashed circular line was multiplied by 30 times relative to that inside the circular line. The patterns b, d, and e were obtained with the in-house SAXS apparatus, while the patterns a and c were obtained with the synchrotron radiation SAXS apparatus.

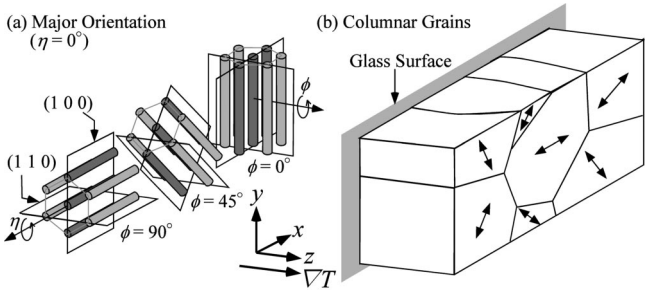

Figure 3. (a) 3-dimensional model for the orientation of hex-cyl developed for the low mobility system YM-1 under the moving ∇T field with $R = 25$ nm/s. (b) "Columnar" grain of hex-cyl. The arrow marked in the grain represents orientation of the cylinder axis. Each grain having a fixed orientation of hex-cyl with respect to ϕ grows along the z-axis.

in the case of $R = 500$ nm/s (part e), the (100) diffraction did not show the specific six-point diffraction pattern but rather show a circular pattern with almost no azimuthal angle (μ) dependence, except for a slightly larger intensity at $\mu = 0$ and 180°. The higher order peaks from (110) and (200) also exhibit the same characteristic as that of (100) diffraction. Similarly to the case of the low mobility system YM-1, there is an upper limit of R to induce the specific texture and orientation for the high mobility system SI-1/HI(95/5) too. However, the upper limit obviously depends on the mobility of bcps; the higher the mobility is, the larger is the upper limit of R.

A comparison between parts a and c of Figure 2 enables us to elucidate the difference in the regularity of lattice structure of hex-cyl in the low and high mobility system. In Figure 2a, the diffraction spots up to (110) plane are observed, while in Figure 2c, the diffraction spots up to (300) plane are discerned. This difference indicates that the lattice regularity is higher in the high mobility system SI-1/HI(95/5) than in the low mobility system YM-1. The same difference can be observed in between parts b and e of Figure 2, both of which exhibit nearly random orientation of hex-cyl. While the scattering only from (100) plane is observed in Figure 3b, the scattering from (200) and (210) plane as well are observed in Figure 3e.

3.3. Positional Dependence of 2D-SAXS Patterns along the ∇T Direction. We investigated the positional dependence of 2D SAXS pattern along the Oz axis for the low and high mobility systems zone-heated with the smallest moving rate, $R = 25$ nm/s and $R = 75$ nm/s, respectively. We found that all 2D SAXS patterns had the typical features inherent in hex-cyl developed via the zone-heating process over the observed z-range $0.2 \leq z/\text{mm} \leq 2.0$, as separately shown in the Supporting Information (Supporting Information 2, see Figures S3 and S4). Therefore the specific orientation of hex-cyl inherent in the zone heating is maintained over the macroscopic length scale even for the low mobility system.

4. Discussion

4.1. Orientation of Cylinders in the Low Mobility System. The SAXS patterns in q_yq_z, q_xq_z, and q_xq_y plane for the zone-heated low mobility system YM-1 with $R = 25$ nm/s have the same features as those for the high mobility system SI-1/HI(95/5) with $R = 75$ nm/s previously reported,[1] as shown in Supporting Information 1 (see Figures S1 and S2), except for the splitting of the equatorial diffraction spots. Thus we can conclude that the same orientation of hex-cyl as that in the case of SI-1/HI(95/5) was developed in the case of YM-1 also. Figure 3 schematically presents a structure model for hex-cyl developed commonly for YM-1 with $R = 25$ nm/s and for SI-1/HI(95/5) with $R = 75$ nm/s. Figure 3a shows a major orientation of hex-cyl, in which one of the three (100) planes is perpendicular to the ∇T direction and parallel to the glass surface; the cylinder axis is confined to the plane parallel to the xy plane but is randomly oriented around the Oz axis. That is, when the rotational angle of cylinder axis around the ∇T axis is defined by ϕ, ϕ takes uniform values from 0° to 180°. It should be noted that the low mobility system also had the minor orientation of hex-cyl, where one of the three (110) planes is perpendicular to the ∇T direction as illustrated in part c of Figure 14 in ref 1 for the high mobility system. The major orientation and the minor orientation are different with respect to the rotational angle η around the cylinder axis by 30°: If the major orientation has $\eta = 0°$, then the minor orientation has $\eta = 30°$ as elucidated previously.[1]

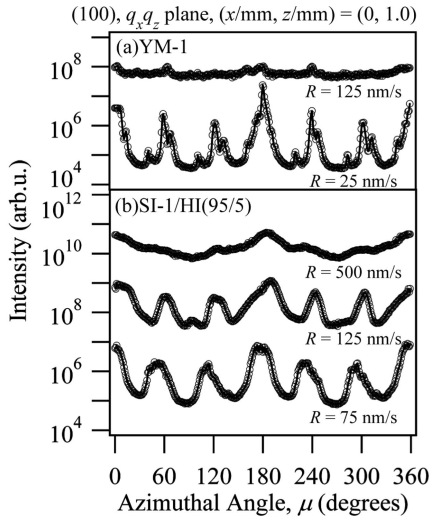

Figure 4. Effects of R on μ-dependence of the (100) diffraction intensity in q_xq_z plane plotted in semilog plot (a) for the low mobility system YM-1; The data for $R = 125$ nm/s is multiplied by 10^6 with respect to the data for $R = 25$ nm/s, and those (b) for the high mobility system SI-1/HI(95/5); The data for $R = 125$ and 500 nm/s are multipled by 10^5 and 10^7 with respect to the data for $R = 75$ nm/s, respectively. The intensity was multiplied in order to avoid an overlap of the curves. The data were obtained from Figure 2a−e.

As explained in our previous paper,[1] the moving ∇T field involves the glass-surface-induced ordering of hex-cyl and the grain having a fixed orientation of hex-cyl with respect to ϕ continues to grow along the Oz axis as long as its growing front faces a sufficiently wide area of disorder phase, while an impingement of neighboring grains occurs in the direction perpendicular to the z axis, as shown in Figure 3b. We designated such grains as "columnar" grain[1] for the sake of convenience from a viewpoint that the grain should have a shape extended along the Oz axis, though the grain shape is not necessarily columnar. The arrow marked in the grain represents orientation of the cylinder axis (or director in the terminology of liquid crystals). The different grains have different director orientations, resulting in a uniform rotational angle with respect to ϕ on a statistical average.

4.2. Effect of Moving Rate on Orientation of Hex-Cyl. Let us now discuss the moving-rate dependence on the texture and orientation of hex-cyl. Figure 4 shows the μ-dependence of the (100) diffraction intensity in q_xq_z plane shown in Figure 2. The parts a and b correspond to the low mobility system YM-1 and the high mobility system SI-1/HI(95/5), respectively. First, we focus on part a. In the case of $R = 25$ nm/s, the μ-dependence quantitatively shows the characteristic of the six-point diffraction pattern with enhanced intensity for the two points at $\mu = 0°$ and 180°, reflecting the orientation of hex-cyl characteristic of the zone-heating process as already discussed in section 4.1. On the other hand, in the case of $R = 125$ nm/s, the (100) diffractions in Figure 2b become almost independent of μ, as more quantitatively shown in Figure 4a, indicating 3-dimensionally random orientation of hex-cyl. At $R = 25$ nm/s, the surface-induced ordering occurs from the glass surface or from the surface of as-grown, well-aligned hex-cyl, so that the microdomain structure has the characteristic orientation and texture. On the other hand, at $R = 125$ nm/s, the ordering from bulk of supercooled disordered melt occurs with little influence of the surfaces, resulting in the randomly oriented microdomain structure.

When we focus on the high mobility system SI-1/HI(95/5), discussions similar to those for the low mobility system YM-1 can be applied for Figures 2c−e and Figure 4b. In the case of $R = 75$ and 125 nm/s, the (100) diffraction gives the characteristics six-point patterns with enhanced intensity for the two points at $\mu = 0$ and 180° as shown in Figures 2 and 4b as well, indicating that the same characteristic orientation and grain of hex-cyl as shown in Figure 3 were developped in the specimen. On the other hand, in the case of $R = 500$ nm/s, the (100) diffraction has only a weak μ-dependence as shown in Figures 2 and 4b, though there are broad peaks at $\mu = 0$ and 180° with shoulders at $\mu = 60$, 120, 240, and 300°, indicating an increased degree of orientation distribution of hex-cyl and apparent loss of the macroscopic orientation achieved by $R = 75$ nm/s. These results are essentially the same as those of the low mobility system YM-1.

Let us now compare the results of the low mobility system YM-1 and those of the high mobility system SI-1/HI(95/5) at the same R, which is also one of the objectives of this study. When the results of YM-1 and SI-1/HI(95/5) at the same moving rate of $R = 125$ nm/s are compared, there is no apparent macroscopic orientation in the low mobility system of YM-1 (Figures 2 and 4a), while there is the characteristic orientation in the high mobility system of SI-1/HI(95/5) (Figures 2 and 4b). This difference in orientation of hex-cyl is due to the difference in mobility of the two bcps. In the system of YM-1, the mobility is low so that the growth rate G for the hex-cyl grains may be smaller than R, leaving supercooled disordered melt phase behind the moving ∇T front, hence resulting in random nucleation and growth and random orientation of hex-cyl. On the other hand, in the system of SI-1/HI(95/5), the mobility is large, and hence $G \geq R$ so that bcps can achieve the directed ordering in the slitlike space. Moreover, the upper limit of R for YM-1 (25 nm/s) is much smaller than that of SI-1/HI(95/5) (125 nm/s). Therefore the rate of grain growth of the ordered phase in the system of SI-1/HI(95/5) can be estimated to be higher by about 5 times than that in the system of YM-1. This difference is at least partially due to the difference in mobility of bcps.

4.3. Positional Dependence of Orientation of Hex-Cyl along ∇T Direction. In this section we shall quantitatively analyze the positional dependence of the orientation of hex-cyl along ∇T direction for the low mobility system YM-1 zone-heated with $R = 25$ nm/s, because this has not been quantitatively analyzed yet. Then we shall compare the results with the result obtained for the high mobility system SI-1/HI(95/5) zone-heated with $R = 75$ nm/s. For this purpose we quantitatively compared the 2D SAXS patterns in q_xq_z plane at various z values for these two systems (see Figures S3 and S4 in Supporting Information 2).

Figure 5 shows the μ-dependence of the (100) diffraction intensity for YM-1 taken at various z values. The data show the 6-fold symmetry with respect to μ up to the largest z, as found in the case of the high mobility system SI-1/HI(95/5) (see Figure 9a in ref 1). The μ-dependence of the diffraction intensity for YM-1 is sharper than that of SI-1/HI(95/5). This trend can be clearly seen when the z-dependence of the half-width at half-maximum (HWHM) of the diffraction peak at $\mu = 180°$ (σ_{180}) as shown in Figure 6a ($\sigma_{180} = 1.4-5.0$ degrees for YM-1) is compared with that for SI-1/HI(95/5) ($\sigma_{180} = 4.4-9.1$ degrees) as shown in Figure 9b in ref 1. These results indicate that the macroscopically well oriented hex-cyl can be created even for the low mobility system as long as R is sufficiently small.

We quantitatively evaluated the orientation distribution of hex-cyl with respect to the angle η and estimated the weight fraction of the major orientation, P_{major}, according to the method given in our previous paper,[1] for YM-1 zone-heated with $R = 25$ nm/s. P_{major} values thus evaluated were plotted as a function of the distance z from the glass surface in Figure 6b. All the

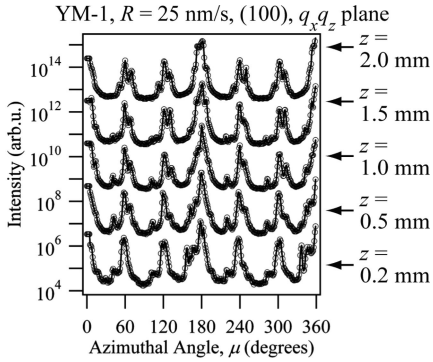

Figure 5. μ-dependence of the (100) diffraction intensity on the $q_x q_z$ plane measured by varying the incident beam position z for the low mobility system YM-1. The intensity data at z/mm = 0.2 are actual values, and other data were shifted up vertically by 2 order of magnitudes relative to the intensities immediately below in order to avoid an overlap of the curves.

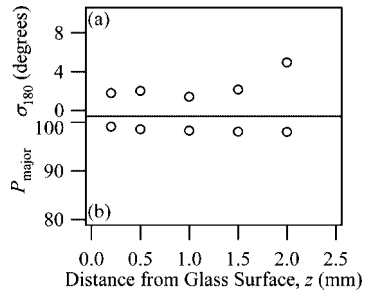

Figure 6. Z-dependence of the half-width at half-maximum (σ_{180}) of the (100) diffraction peak with respect to μ at μ = 180° and (b) Z-dependence of the weight fraction of major orientation (P_{major}) for YM-1 at R = 25 nm/s.

values for P_{major} in the system of YM-1 were in the range from 98% to 99% and almost constant in the observed z-range. The values are comparable with those for the system of SI-1/HI(95/5), which are in the range from 95% to 98% as shown in Figure 15 in ref 1. These results also suggest that we can control macroscopically the orientation of hex-cyl over a large distance from the glass surface by using a sufficiently small R.

It is interesting to note that the high mobility system ordered at R = 75 nm/s has more perfectly ordered hex-cyl lattice (as revealed by Figure 2) but less perfect orientation (as revealed by comparisons of Figures 5 and 6 with Figures 9 and 15 in ref 1) than the low mobility system ordered at R = 25 nm/s. The orientation of the high mobility system will be further improved when R is reduced without effects of thermal degradation.

4.4. Effects of Glass Surface. In this section we shall discuss effects of glass surfaces on the orientation. The glass surface used for the low mobility system YM-1 is different from that used for the high mobility system SI-1/HI(95/5). In the former case the PS-coated glass was used, while in the latter case the bare glass surface was used.

Figure 7a, which represents the case of applying the zone heating to YM-1, schematically indicates a possible packing of polymer chains near the PS-coated glass surface. In this case, PS block chains, which form the matrix phase of PI cylinders, contact to PS coating layer. The PS brush chains on the glass surface will enhance wetting of the PS block chains emanating from the PI cylinders, simply because the interfacial tension of the PS bcp chains and the PS brush chains is lower than that of the PS bcp chains and the bare glass surface. When the bare glass surface was used in the zone heating process for YM-1 at R = 25 nm/s and $|\nabla T|_{eff}$ = 22 °C/mm, we found almost the same results as in the case of the PS-coated glass at the same

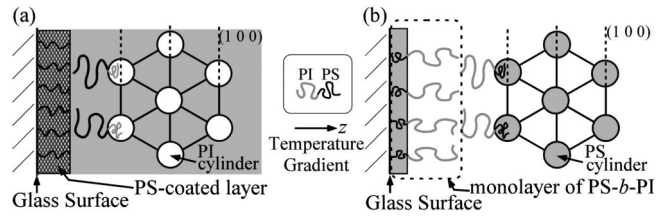

Figure 7. Schematic illustrations for the packing of polymer chains near the glass surface in the case of PS-rich bcp system on the PS coated glass surface (a) and the PI-rich bcp system on the bare glass (b).

values of R and $|\nabla T|_{eff}$. Some results obtained with the bare glass are presented as Supporting Information (Supporting Information 3, see Figures S5 and S6). When the bare glass surface is used in the zone heating process of the PI-rich bcp system (the high mobility system), PI block chains may contact with the glass surface. Since the interfacial tension between the bare glass surface and PI block chains is higher than that between the surface and PS block chains as elucidated in section 4.4 of ref 1, a part of the bcps is expected to form a monolayer at the interface between bcps and the glass surface as shown in Figure 7b in which the layer on the glass side is occupied by the PS-block brush chains and the layer on the interior side of the specimen is occupied by the PI-block chains so as to minimize the interfacial tension between the bare glass and the PI block chains.

5. Concluding Remarks

The moving ∇T field imposed on the ordering process of the cylinder-forming bcps from disordered melt was discovered to develop a unique "columnar" texture having a special texture and orientation of hex-cyl in our previous paper.[1] This piece of evidence was further confirmed by the present experimental work which explored effects of changing mobility of the bcps and moving rate of ∇T. We elucidated that there is an upper limit of the moving rate R to induce the unique texture and orientation of hex-cyl and that the upper limit becomes larger with increasing the mobility of the bcps. The slow moving rate is important in order to develop the columnar grains of hex-cyl with the specific orientation.

Acknowledgment. Part of the SAXS measurements in this work was conducted under approval of the SPring-8 (2005A 0690).

Appendix

In order to compare the mobility of the PS-rich bcp system YM-1 with that of the PI-rich bcp system SI-1/HI(95/5) during ordering process from disordered state, we estimate the diffusion coefficients of both systems at the respective T_{ODT}s.

We first calculated the diffusion coefficient of homo-PS (designated as h-PS_{YM-1}), which has the same degree of polymerization as YM-1, at T_{ODT} of YM-1, and the diffusion coefficient of homo-PI (designated as h-PI_{SI-1}), which has the same degree of polymerization as SI-1, at T_{ODT} of SI-1/HI(95/5). The diffusion coefficients of h-PS_{YM-1} and h-PI_{SI-1} designated as $D_{h\text{-}PS,147}$ and $D_{h\text{-}PI,178}$, respectively, can be calculated to be $D_{h\text{-}PS,147} = 3.4 \times 10^{-13}$ cm^2/s and $D_{h\text{-}PI,178} = 1.1 \times 10^{-9}$ cm^2/s, as will be described immediately below. $D_{h\text{-}PS,147}$ was estimated by using the reported data[12] on diffusion coefficients of PS as a function of degree of polymerization at 212 °C. Then the value at 212 °C was converted to that at 147 °C by using the WLF equation on temperature dependence of the diffusion coefficient D of PS with the glass transition temperature T_g of 373 K and WLF parameters[13] C_{1g} = 13.7, C_{2g} = 57:

$$\log\left(\frac{D_g}{D}\right) = -\frac{C_{1g}(T - T_g)}{C_{2g} + (T - T_g)} \quad (1)$$

Here D and D_g are diffusion coefficients at T and T_g, respectively. $D_{\text{h-PI},178}$ was assessed by using the reported data[14] on temperature dependence of diffusion coefficients of homo-PI having a molecular weight of 2.12×10^4 and then by using reptation model in order to convert the value for molecular weight of 2.12×10^4 to that of h-PI_{SI-1}.

Next, we evaluate the diffusion coefficients of YM-1 at 147 °C, $D_{\text{YM-1},147}$, and SI-1 at 178 °C, $D_{\text{SI-1},178}$ from the values $D_{\text{h-PS},147}$ and $D_{\text{h-PI},178}$, respectively, by taking into consideration that YM-1 and SI-1 are the bcps containing PI and PS, respectively. D can be expressed in the Rouse model as

$$D = \frac{k_B T}{N\zeta_{\text{eff}}} \quad (2)$$

and in the reptation model[15] as

$$D = \frac{k_B T}{N\zeta_{\text{eff}}}\left(\frac{4N_e}{15N}\right) \quad (3)$$

where k_B is the Boltzmann constant, N is the degree of polymerization, N_e is the entanglement spacing, and ζ_{eff} is the effective monomeric friction factor at T. ζ_{eff} depends on the composition and temperature. On the basis of eqs 2 and 3, $D_{\text{YM-1},147}$ and $D_{\text{SI-1},178}$ at T_{ODT} can be expressed by using the diffusion coefficients of the corresponding homopolymers having the same N at the same T, $D_{\text{h-PS},147}$ and $D_{\text{h-PI},178}$, respectively, if N_e for each bcp has the same value as that of the corresponding homopolymer,

$$D_{\text{YM-1},147} = D_{\text{h-PS},147}\left(\frac{\zeta_{\text{eff,YM-1},147}}{\zeta_{\text{eff,h-PS},147}}\right)^{-1} \quad (4)$$

$$D_{\text{SI-1},178} = D_{\text{h-PI},178}\left(\frac{\zeta_{\text{eff,SI-1},178}}{\zeta_{\text{eff,h-PI},178}}\right)^{-1} \quad (5)$$

where $\zeta_{\text{eff,YM-1},147}$ and $\zeta_{\text{eff,SI-1},178}$ are ζ_{eff} for YM-1 at 147 °C and SI-1 at 178 °C, respectively, and $\zeta_{\text{eff,h-PS},147}$ and $\zeta_{\text{eff,h-PI},178}$ are ζ_{eff} for h-PS_{YM-1} at 147 °C and h-PI_{SI-1} at 178 °C, respectively. Equations 4 and 5 are valid both for the Rouse model and the reptation model.[15]

Lodge and co-workers[16] reported that the composition and temperature dependence of ζ_{eff} can be assessed through the composition and temperature dependence of $\Delta T = T - T_{g,\text{eff}}$, where $T_{g,\text{eff}}$ is T_g of polymer chains in the disordered state in the case of bcp or T_g itself in the case of pure PS or PI. According to their report, $T_{g,\text{eff}}$ can be approximated by the Fox equation, and ζ_{eff} monotonously decreases with ΔT. The Fox equation[17] is

$$\frac{1}{T_{g,\text{eff}}} = \frac{w_{PS}}{T_{g,PS}} + \frac{w_{PI}}{T_{g,PI}} \quad (6)$$

where w_i and $T_{g,i}$ (i = PS and PI) are the weight fraction and the T_g of the ith component, respectively. In their paper, ζ_{eff} values were plotted as a function of ΔT, so that we can estimate ζ_{eff} for each polymer by calculating ΔT. ΔT of each polymer at T_{ODT} is calculated as 47 K for h-PS_{YM-1}, 119 K for YM-1, 210 K for SI-1, and 250 K for h-PI_{SI-1} from the reported T_g of homo-PS (373 K) and homo-PI (201 K)[18,19] and eq 6. Thus, we can estimate ζ_{eff}s from these values of ΔT and hence $D_{\text{YM-1},147}$ and $D_{\text{SI-1},178}$ from the evaluated values of ζ_{eff}s, $D_{\text{h-PS},147}$ and $D_{\text{h-PI},178}$ by using eqs 4 and 5, respectively. The results are $D_{\text{YM-1},147} = 2.1 \times 10^{-11}$ cm^2/s and $D_{\text{SI-1},178} = 3.0 \times 10^{-10}$ cm^2/s, indicating the diffusion coefficient of YM-1 is smaller than those of SI-1 and SI-1/HI(95/5). Therefore it is reasonable that we treated YM-1 as the low mobility system and SI-1/HI(95/5) as the high mobility system.

Supporting Information Available: Supporting Information 1, text discussing the texture and orientation of hex-cyl in low mobility system, including Figure S1, 2D-SAXS patterns obtained for the low mobility system YM-1, and Figure S2, μ-dependence of the patterns shown in Figure S1, Supporting Information 2, text discussing the positional dependence of 2D-SAXS patterns along the ∇T direction, including Figure S3, positional dependence of 2D-SAXS patterns with respect to z for the low mobility system, and Figure S4, positional dependence of 2D-SAXS patterns with respect to z for the high mobility system, and Supporting Information 3, text discussing the application of zone heating method to YM-1 with bare glass, including Figure S5, 2D-SAXS pattern obtained for the specimen of YM-1 zone-heated with the bare glass, and Figure S6, μ-dependence of the (100) diffraction intensity on the q_xq_z plane measured by varying the incident beam position z for the specimen of YM-1 zone-heated with the bare glass. This information is available free of charge via the Internet at http://pubs.acs.org.

References and Notes

(1) Mita, K.; Tanaka, H.; Saijo, K.; Takenaka, M.; Hashimoto, T. *Macromolecules* **2007**, *40*, 5923.
(2) Hashimoto, T.; Kawamura, T.; Harada, M.; Tanaka, H. *Macromolecules* **1994**, *27*, 3063.
(3) Hashimoto, T.; Tanaka, H.; Hasegawa, H. *Macromolecules* **1990**, *23*, 4378.
(4) The effective width is expected to be much narrower than that estimated above because the growth of the grain occurs dominantly in the narrow temperature range where the growth rate is a maximum.
(5) Philipse, A. P.; Vrij, A. J. *Colloid Interface Sci.* **1989**, *128*, 121.
(6) Bodycomb, J.; Funaki, Y.; Kimishima, K.; Hashimoto, T. *Macromolecules* **1999**, *32*, 2075.
(7) In ref 1, we described that we used the poly(ethylenetelephtarate) (PET) sheets in order to confine 2 mm thick film. This is a mistake. Actually we used polyimide sheets called Kapton.
(8) Hashimoto, T.; Suehiro, S.; Shibayama, M.; Saijo, K.; Kawai, H. *Polym. J.* **1981**, *13*, 501.
(9) Fujisawa, T.; Inoue, K.; Oka, T.; Iwamoto, H.; Uraga, T.; Kumasaka, T.; Inoko, Y.; Yagi, N.; Yamamoto, M.; Ueki, T. *J. Appl. Crystallogr.* **2000**, *33*, 797.
(10) There is one difference between the apparatus used in this paper and that used in ref 1. The difference is the size of the two pin holes used in the camera. We chose the pin holes having diameter 0.3 mm in this experiment, while the pin holes had diameter 0.5 mm in the ref 1. The beam size at the sample surface was circular shape with the radius of 0.3 mm.
(11) The exposure times to take 2D SAXS patterns were 43200, 7200, and 43200 s, when incident beam was irradiated along the Ox, Oy, and Oz directions, respectively.
(12) Antonietti, M.; Fölsch, K. J.; Sillescu, H. *Makromol. Chem.* **1987**, *188*, 2317.
(13) Ferry, J. D. *Viscoelastic Properties of Polymers*, 3rd ed.; Wiley: New York, 1980.
(14) Ehlich, D.; Takenaka, M.; Hashimoto, T. *Macromolecules* **1993**, *26*, 492.
(15) Doi, M.; Edwards, S. F. *The Theory of Polymer Dynamics*; Oxford Univ. Press: New York, 1986.
(16) Chapman, B. R.; Hamersky, M. W.; Milhaupt, J. M.; Kostelecky, C.; Lodge, T. P.; Meerwall, E. D.; Smith, S. D *Macromolecules* **1998**, *31*, 4562.
(17) Fox, T. G. *Bull. Am. Phys. Soc.* **1956**, *1*, 123.
(18) Schrader,D. In *Polymer Handbook*, 4th ed.; Brandrup, J., Immergut, E. H., Grulke, E. A., Eds.; John Wiley & Sons Inc.: New York, 1999; p V-91.
(19) Furuta, I.; Kimura, S.; Iwama, M. In *Polymer Handbook*, 4th ed.; Brandrup, J., Immergut, E. H., Grulke, E. A., Eds.; John Wiley & Sons Inc.: New York, 1999; p V-5.

MA8001998